

Cooperative roles of glucose and asparagine-linked glycosylation in T-type calcium channel expression

Joanna Lazniewska¹ · Yuriy Rzhpetsky¹ · Fang-Xiong Zhang² · Gerald W. Zamponi² · Norbert Weiss¹

Received: 29 June 2016 / Revised: 4 September 2016 / Accepted: 7 September 2016 / Published online: 23 September 2016
© Springer-Verlag Berlin Heidelberg 2016

Abstract T-type calcium channels are key contributors to neuronal physiology where they shape electrical activity of nerve cells and contribute to the release of neurotransmitters. Enhanced T-type channel expression has been causally linked to a number of pathological conditions including peripheral painful diabetic neuropathy. Recently, it was demonstrated that asparagine-linked glycosylation not only plays an essential role in regulating cell surface expression of Ca_v3.2 channels, but may also support glucose-dependent potentiation of T-type currents. However, the underlying mechanisms by which N-glycosylation and glucose levels modulate the expression of T-type channels remain elusive. In the present study, we show that site-specific N-glycosylation of Ca_v3.2 is essential to stabilize expression of the channel at the plasma membrane. In contrast, elevated external glucose concentration appears to potentiate intracellular forward trafficking of the channel to the cell surface, resulting in an increased steady-state expression of the channel protein at the plasma membrane. Collectively, our study indicates that glucose and N-glycosylation act in concert to control the expression of Ca_v3.2 channels, and that alteration of these mechanisms may contribute to the altered expression of T-type channels in pathological conditions.

Keywords Calcium channel · T-type channel · Ca_v3.2 · Glucose · N-glycosylation · Trafficking

✉ Norbert Weiss
weiss@uochb.cas.cz

¹ Institute of Organic Chemistry and Biochemistry, Ion Channels and Diseases group, Academy of Sciences of the Czech Republic, Prague, Czech Republic

² Department of Physiology and Pharmacology, Cumming School of Medicine, University of Calgary, Calgary, Canada

Introduction

Low-voltage-activated T-type calcium (Ca²⁺) channels including Ca_v3.1, Ca_v3.2, and Ca_v3.3 channel isoforms, are broadly expressed throughout the nervous system where they contribute to complex yet fundamentally essential neuronal functions [24, 31]. T-type channels are uniquely suited to operate near the resting membrane potential of nerve cells where they generate rebound burst of action potentials that shape various forms of neuronal rhythmogenesis [3, 4, 6]. In addition, they associate with and control the activity of a number of potassium channels to fine tune neuronal excitability [34]. Besides, to control the excitability of nerve cells, T-type channels also directly contribute to synaptic transmission where they trigger the release of neurotransmitter by virtue of their biochemical association with the vesicular release machinery [38–40]. The essential contribution of T-type channel to the nervous system is further exemplified by the occurrence of a number of pathological conditions linked to the alteration of T-type channel function [32, 43]. For instance, alteration of T-type channel expression has been reported in a number of chronic pain conditions [36, 42] including peripheral painful diabetic neuropathy [8, 10–12]. There is, therefore, increasing interest in identifying the underlying cellular mechanisms responsible that control expression of T-type channels.

A number of signaling pathways regulating the expression level of T-type channels have been reported and include ubiquitination [9] and Stac adaptor proteins [27]. In addition, asparagine (N)-linked glycosylation has also emerged as a fundamental mechanism to control the functional expression of ion channels [14]. N-linked glycosylation relies on the covalent attachment of a sugar molecule oligosaccharide (glycan) to an asparagine (N) residue within a consensus site N-x-S/T in the target protein. Although N-linked glycosylation is essential for the proper folding of newly synthesized

polypeptide chains [18], a role in the sorting, trafficking, and function of ion channels at the cell surface has emerged. For instance, we and others have demonstrated that N-glycosylation of $Ca_v3.2$ is critical for the functional expression and modulation of the channel at the cell surface [22, 23, 37]. In addition, it was proposed that N-glycosylation might support glucose-dependent up-regulation of $Ca_v3.2$ channels that occurs in the course of mellitus diabetes [23, 37].

Although our previous studies implicated a role for both glucose and N-glycosylation in the expression of T-type channels, the relative contribution or interaction mechanisms between glucose and N-glycosylation remain unknown. Here, we report a differential contribution for glucose and N-glycosylation in the expression of T-type channels at the plasma membrane. Using glycosylation-deficient $Ca_v3.2$ channels, we show that N-linked glycosylation increases the steady-state expression of T-type channels at the cell surface by stabilizing the channel protein in the plasma membrane. In contrast, we demonstrate that elevated external glucose level increases intracellular forward trafficking of the channel to the plasma membrane. Our finding thus provide new insights into the molecular mechanisms of T-type channel expression and reveal that glucose and N-glycosylation use different routes but work in concert to control the density of T-type channels expressed at the cell surface.

Materials and methods

Plasmid cDNA constructs

The human wild-type HA-tagged $Ca_v3.2$ construct (HA- $hCa_v3.2^{WT}$) [7] and glycosylation-deficient $hCa_v3.2$ mutants used in this study were previously described [37, 38]. Briefly, the HA- $hCa_v3.2^{WT}$ construct was used as a template for mutation of the consensus N-glycosylation sites by substituting the asparagine residues N192, N271, N1466, and N1710 with glutamine (Q) residues by site-directed mutagenesis using the QuikChange IITM Site-Directed Mutagenesis Kit (Agilent Technologies Inc.). Glutamine was chosen because of its structural similarity with asparagine residues, differing only by one methyl group in the amino acid side chains, which is consequently expected to preserve the local charge distribution within the protein and the secondary structure of the channel. To generate the amino-terminally mCherry-tagged $Ca_v3.2$ constructs, the HA- $hCa_v3.2^{WT}$ template was used to amplify by PCR the full-length $Ca_v3.2$ using the following primers: 5'-AATCCTCGAGCCATGACCGAGGGC-3' (forward) and 5'-ACTCAAGCTTCTACACGGGGTCATCTGC-3' (reverse), and the PCR product was inserted into the XhoI/HindIII sites of pEGFP-C1 vector. The GFP encoding sequence was then removed by cutting into NheI/XhoI sites and replaced by the mCherry encoding sequence amplified using the following

primers: 5'-TCCGCTAGCGCTACCGGTCGCCACCA TGGTGAGCAAGGGCGAGGAGGATAACAT-3' (forward) and 5'-TACTCGAGATCTGAGTCCGGACTTGTACAGCT CGTCCATGCCCCGGT-3' (reverse). To generate the complementary DNA (cDNA) constructs encoding for amino-terminal Myc-tagged $hCa_v3.2$ transmembrane domains, the wild-type HA-tagged $hCa_v3.2$ or HA-tagged $hCa_v3.2$ N192Q/N1466Q constructs were used as template to amplify by PCR the sequence corresponding to domains I and III using the following primers: 5'-ATCTCGAGATTCCGAGAGCCCGG-3' (forward) and 5'-CTTAAGCTTTCACACGTA CTTCAGCAGCTCTT-3' (reverse) and 5'-ATCTCGAGATACCAAGTGCCGCGAT-3' (forward) and 5'-GAGAAGCTTTCACCTGCGCCTCTCTCTAG-3' (reverse), respectively, and the PCR products were subcloned in the XhoI/HindIII sites of the pEGFP-C1 vector. The GFP encoding sequence was then removed by cutting into NheI/XhoI sites and replaced by the Myc encoding sequence using the products of hybridization of the following primers: 5'-TCCGCTAGCGCTACCGGTCGCCACCATGGAAC AAAAATCATCTCAGAAGAGGATCTGGCTCGAGTAG-3' (forward) and 5'-CTACTCGAGCCAGATCCTCTTCTGAG ATGAGTTTTTGTCCATGGTGGCGACCGGTAGCGCT AGCGGA-3' (reverse). To generate the pEGFP-ER construct, the pDsRed2-ER vector (Clontech) was used to amplify by PCR the ER targeting sequence of calreticulin using the following primers: 5'-TCCGCTAGCATGCTGCTATCCGTGCC GTTGCTGCTCGGCCTCTCGGCCTGGCCGTCGCCCC ACCGGTCGCC-3' (forward) and 5'-GGCGACCGGTCCGG CGACGGCCAGGCCGAGGAGGCCGAGCAGCA ACGGCACGGATAGCAGCATGCTAGCGGA-3' (reverse), and the PCR product was cloned in the NheI/AgeI sites of the pEGFP-C1 vector. Similarly, the pDsRed-Monomer-Golgi vector (clontech) was used as a template to amplify by PCR the sequence encoding for the N-terminal 81 amino acids of the human beta 1,4-galactosyltransferase using the following primers: 5'-TCCGCTAGCATGAGGCTTCGGGAGCC GCTCCTG-3' (forward) and 5'-GGCGACCGGTGGAT CCTTGGCCCCCTCCGGTCCGG-3' (reverse), and the PCR product was cloned into the NheI/AgeI sites of pEGFP-C1 vector to generate the pEGFP-ER construct. All final constructs were verified by sequencing of the full-length cDNAs.

Cell culture and heterologous expression

Human embryonic kidney tsA-201 cells were grown in DMEM medium containing either physiological glucose concentration (5 mM and referred as low glucose condition) or elevated glucose level (25 mM and referred as high glucose condition), supplemented with 10 % fetal bovine serum and 1 % streptomycin/penicillin (all media from Invitrogen), and maintained under standard conditions at 37 °C in a humidified atmosphere containing 5 % CO₂. Cells were plated out onto

60-mm dishes and transiently transfected using the calcium/phosphate method.

Immunostaining

Immunostaining of HA-tagged hCa_v3.2-expressing cells was performed 48 h after transfection. Cells were harvested using a non-enzymatic EDTA-based chelating agent (Versen™), and seeded on poly-L-lysine-coated glass coverslips. For surface staining, cells were incubated for 30 min at 37 °C with a primary mouse anti-HA antibody (Abcam) diluted in DMEM at 1:1000, washed three times with PBS, and fixed for 7 min in 4 % formaldehyde. Then, cells were washed three times in PBS following by 45 min blocking step in 5 % FBS, and samples were incubated for 1 h with an Alexa Fluor488-conjugated secondary anti-mouse antibody (Jackson ImmunoResearch) diluted at 1:1000 in the blocking buffer. After washing three times, coverslips were transferred onto a microscopic slide using ProLong Gold mounting medium (Life Technologies). For total staining, cells were fixed for 15 min in formaldehyde, and permeabilized with 0.2 % Triton-X100 for 10 min before to perform the immunostaining. Confocal images were acquired at low magnification with a Zeiss LSM780 microscope, and the field fluorescence intensity was analyzed using ImageJ software from non-permeabilized and permeabilized cells to assess surface and total expression of HA-hCa_v3.2 channels, respectively.

SDS-PAGE and immunoblot analysis

Total cell lysates (50 µg of protein), were separated on 10 % SDS-PAGE and transferred onto PVDF membrane (Millipore). For detection of the myc-tagged fusion proteins, the membrane was incubated overnight (4 °C) with a rabbit primary monoclonal anti-myc antibody (Cell Signaling Technology) diluted at 1:1000. For detection of HA-tagged fusion proteins, the same membrane was stripped in 0.2 % glycine, 1 % SDS solution (pH 2.0) for 30 min, and then re-probed overnight (4 °C) with a rat primary monoclonal anti-HA antibody (Roche) diluted at 1:2000. After incubation with primary antibodies, the membrane was washed in PBS/Tween-20 buffer, and incubated 1 h with the corresponding secondary HRP-conjugated antibody (Jackson ImmunoResearch) diluted at 1:10,000.

Patch-clamp electrophysiology

Patch-clamp recordings were performed 72 h after transfection in the whole-cell configuration of the patch-clamp technique at room temperature (22–24 °C) in a bath solution containing (in millimolar): 5 BaCl₂, 5 KCl, 1 MgCl₂, 128 NaCl, 10 TEA-Cl, 10 D-glucose, 10 4-(2-hydroxyethyl)-1-piperazineethanesulfonic acid (HEPES) (pH 7.2 with NaOH). Patch pipettes had a

resistance of 2–4 MΩ when filled with a solution containing (in millimolar): 110 CsCl, 3 Mg-ATP, 0.5 Na-GTP, 2.5 MgCl₂, 5 D-glucose, 10 EGTA, and 10 HEPES (pH 7.4 with CsOH). Whole-cell patch-clamp recordings were performed using an Axopatch 200B amplifier (Axon Instruments). Acquisition and analysis were performed using pClamp 10 and Clampfit 10 software, respectively (Axon Instruments).

Ba²⁺ currents were recorded in response to 150-ms-long depolarizing to various potentials applied every 5 s from a holding potential of –100 mV. The linear leak component of the current was corrected online and current traces were digitized at 10 kHz, and filtered at 2 kHz. The voltage dependence of the peak Ba²⁺ current density was fitted with the following modified Boltzmann equation:

$$I(V) = G_{\max} \frac{(V - V_{\text{rev}})}{1 + \exp\left(\frac{V_{0.5} - V}{k}\right)}$$

with $I(V)$ being the peak current amplitude at the command potential V , G_{\max} the maximum conductance, V_{rev} the reversal potential, $V_{0.5}$ the half-activation potential, and k the slope factor. The voltage dependence of the whole-cell Ba²⁺ conductance was calculated using the following modified Boltzmann equation:

$$G(V) = \frac{G_{\max}}{1 + \exp\left(\frac{-(V - V_{0.5})}{k}\right)}$$

with $G(V)$ being the Ba²⁺ conductance at the command potential V .

The steady-state voltage dependence of inactivation of the Ba²⁺ current was determined by measuring the peak current amplitude in response to a 150-ms-long depolarizing step to –20 mV applied after a 5-s-long conditioning prepulse ranging from –105 to –50 mV. The current amplitude obtained during each test pulse was normalized to the maximum at –105 mV and plotted as a function of the prepulse potential. The voltage dependence of the steady-state inactivation was fitted with the following two-state Boltzmann function:

$$I(V) = \frac{I}{1 + \exp\left(\frac{V_{0.5} - V}{k}\right)}$$

with I_{\max} corresponding to the maximal peak current amplitude and $V_{0.5}$ to the half-inactivation voltage.

Internalization studies

For internalization studies, HA-hCa_v3.2-expressing cells were incubated for 30 min at 37 °C with a primary mouse anti-HA antibody (Abcam) diluted in DMEM at 1:1000, washed three

times, and maintained at 37 °C for a variable duration to allow internalization of the channel protein before to be fixed and immunostained as described above.

Fluorescence recovery after photobleaching

Fluorescence recovery after photobleaching (FRAP) was performed at 37 °C on live tsA-201 cells expressing mCherry-tagged hCa_v3.2 channels together with the ER-GFP or Golgi-GFP in order to visualize cell compartments. FRAP was performed using a confocal microscope LSM780 (Zeiss), with a 1.4 aperture 63× oil-immersion objective. The GFP and mCherry fluorescence were excited at 488 and 587 nm, respectively, and fluorescence signals were collected using separate bandpass filters. A region of interest (ROI) for photobleaching was chosen and three pre-bleached images were collected at 2 % laser intensity, following by photobleaching at 80 % laser intensity using six iterations. The recovery of fluorescence was recorded at 2 % laser intensity. Additionally, the fluorescence of a non-bleached background region was monitored. Images were analyzed using ImageJ software. Fluorescence in a given ROI was measured, the background signal was subtracted, and the values were corrected for the non-specific photobleaching in non-bleached ROI. Pre-bleaching fluorescence signals were normalized to 100 %, and post-bleaching signals to 0 %. The normalized fluorescence recovery was plotted as a function of time.

DRG neuron culture and calcium imaging

Dorsal root ganglion (DRG) neurons from 5- to 6-week-old rat were dissociated enzymatically with 4 mg/ml collagenase type 1A (Invitrogen, Thermo Scientific, Waltham, MA); 40 µl/ml papain (Worthington, Lakewood, NJ) at 37 °C for 30 min; and then, 0.1 mg/ml DNase I (Sigma) in F-12 medium (Life Technologies, Grand Island, NY, USA) at 37 °C for 10 min, followed by mechanical trituration with a fire-polished Pasteur pipette. Cells were seeded in 48-well plate and cultured in F-12 medium, supplemented with 10 % (v/v) FBS (HyClone, Thermo Scientific, Pittsburgh, PA), 100 ng/ml nerve growth factor (NGF) (Invitrogen), 2 % N2 (Invitrogen), 2 % B27 (Invitrogen), 1 % L-Glutamine (Sigma) and 1 % penicillin–streptomycin (Invitrogen). High glucose was treated at 24 h after plating and stored for 2 days before carrying on calcium imaging.

Calcium imaging of DRG neurons loaded with fluorescent dyes was performed using a Zeiss LSM510 confocal system (Carl Zeiss Jena GmbH, Jena, Germany). Fluo 4-AM in 1× PBS (5 µM, Thermo Fisher Scientific, Waltham, MA) was loaded for 30 min in the dark at room temperature to measure intracellular Ca²⁺ concentration. Low KCl bath solution containing in millimolar: 5 KCl, 150 NaCl, 2.5 CaCl₂, 1 MgCl₂,

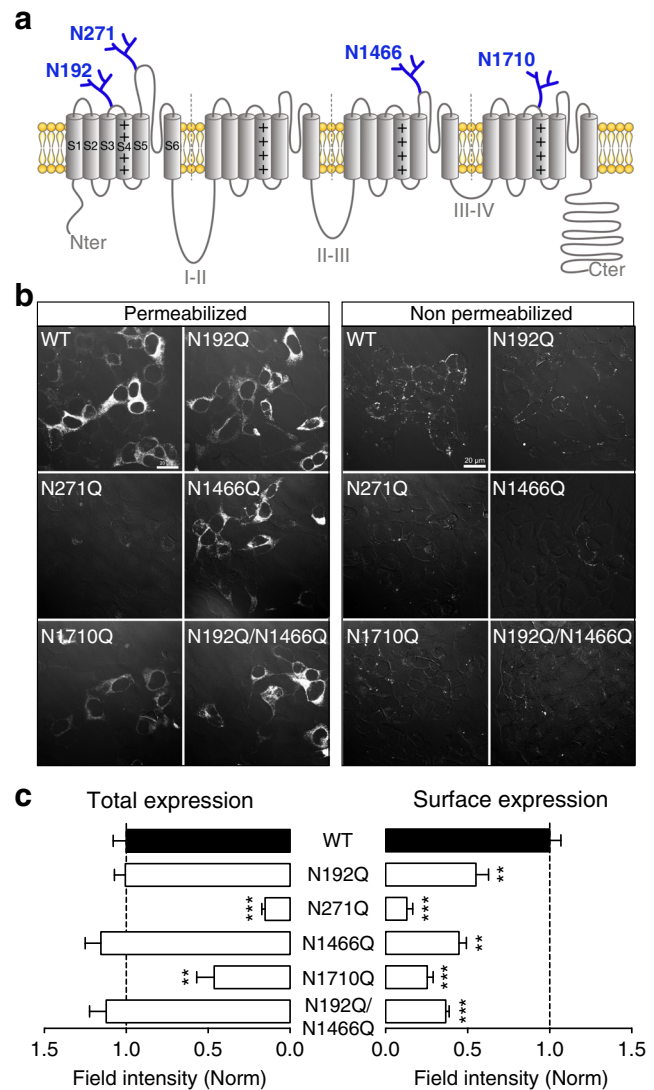
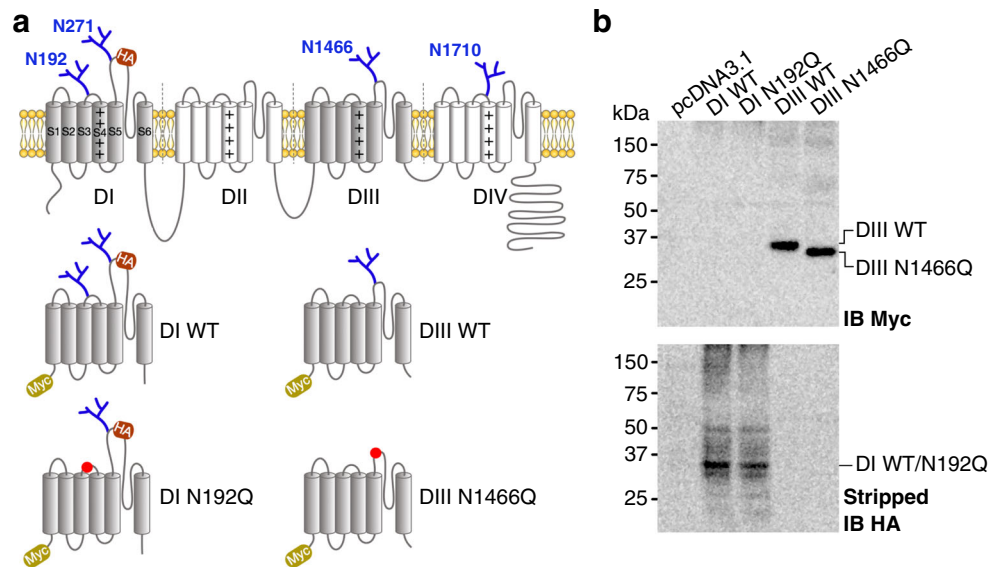


Fig. 1 N-glycosylation controls expression of hCa_v3.2 channels. **a** Schematic representation of canonical N-linked glycosylation loci (in blue) within the scheme of hCa_v3.2 channel structure. **b** Low-magnification confocal images of permeabilized (left panels) and non-permeabilized (right panels) tsA-201 cells expressing wild-type (WT) and glycosylation-deficient HA-tagged hCa_v3.2 channels, and immunostained using a primary anti-HA antibody. **c** Corresponding mean total (permeabilized) and surface (non-permeabilized) expression of HA-hCa_v3.2 channels assessed by field fluorescence intensity measurement. Data are presented as mean ± S.E.M of three to five measurements from independent experiments, and each measurement was obtained by averaging the fluorescence intensity of 10 confocal fields. Data were analyzed by one-way ANOVA with Turkey's posttests; ** $p < 0.01$, *** $p < 0.001$

10 HEPES, and 10 glucose, pH 7.4 and including 10 µM cadmium to eliminate the contribution of HVA channels, and calcium signals were evoked with high KCl (KCl 50, 105 NaCl, 2.5 CaCl₂, 1 MgCl₂, 10 HEPES, and 10 glucose) stimuli. The fluorescence of Fluo 4 was excited using an argon 488-nm laser line, with emitted light collected using an LP505 filter. Ca²⁺ images were taken with a frequency of 0.2 Hz.

Fig. 2 Biochemical indication of N-glycosylation of hCa_v3.2 channels. **a** Schematic representation of the different Myc-tagged constructs used and corresponding to the transmembrane regions I and III of hCa_v3.2. **b** Western blot of wild-type and glycosylation-deficient Myc-tagged hCa_v3.2 domain I (DI WT and DI N192Q) and domain III (DIII WT and DIII N1466Q). The *upper panel* shows the result of the western blot using an anti-Myc antibody. The *lower panel* shows the immunoblot of the same membrane, stripped, and reblotted with an anti-HA antibody



Changes in fluorescence intensity were determined using image analysis software (Zeiss LSM 510, Carl Zeiss Jena GmbH). Intensities were expressed in relation to baseline fluorescence preceding stimulus, resulting in $\Delta F/F$ values.

Statistical analysis

Data values are presented as mean \pm SEM for n experiments. Statistical significance was determined using one-way ANOVA with Turkey's post tests or Student's unpaired t test: * $p < 0.05$, ** $p < 0.01$, and *** $p < 0.001$.

Results

N-linked glycosylation contributes to cell surface expression of hCa_v3.2 channels

The human Ca_v3.2 channel contains four canonical glycosylation sites at asparagine residues N192, N271, N1466, and N1710 (Fig. 1a). In a previous study, we have reported that preventing glycosylation at asparagine N271 and N1710 caused a drastic loss of channel expression, suggesting a role for these glycosylation loci in the folding and/or maturation of the channel protein [37]. In contrast, we have demonstrated that glycosylation at asparagine N192 and N1466 had little influence on the expression of the channel protein per se, but is essential for proper surface and functional expression of the channel. To further assess the role of these two glycosylation loci, we examined surface expression of hCa_v3.2 channels expressed in tsA-201 cells by immunostaining using an exofacial hemagglutinin (HA)-tagged hCa_v3.2 (HA-hCa_v3.2). The expression of HA-hCa_v3.2 wild-type (WT) and glycosylation-deficient N192Q and N1466Q mutants

was quantified from low-magnification images obtained from non-permeabilized and permeabilized cells to assess surface and total expression of the channel, respectively (Fig. 1b). Immunostaining from non-permeabilized cells revealed a 45 % decreased ($p = 0.0056$), 55 % decreased ($p = 0.0012$), and 63 % decreased ($p = 0.0005$) surface expression of N192Q, N1466Q, and N192Q/N1466Q channel mutants, respectively, compared to the surface expression of the wild-type channel (Fig. 1c, right panel). In contrast, the total expression of the glycosylation-deficient channels assessed from permeabilized cells remained unchanged (Fig. 1c, left panel). These results are consistent with our previous observation [37] confirming the validity of our experimental approach used to assess the expression of the channel protein. On the other hand, the total expression of glycosylation-deficient N271Q and N1710Q mutant channels was dramatically decreased compared to wild-type channels, and the surface expression was virtually undetectable, suggesting a role for these glycosylation loci in the biogenesis of the channel protein, and the surface trafficking of these glycosylation-deficient channels was therefore not further analyzed. Considering that preventing glycosylation at asparagine residues N192 and N1466 did not alter total expression of the channel protein, we used the double N192Q/N1466Q mutant channel as a minimal glycosylated form to further analyze the role of N-glycosylation in the trafficking of hCa_v3.2 channels.

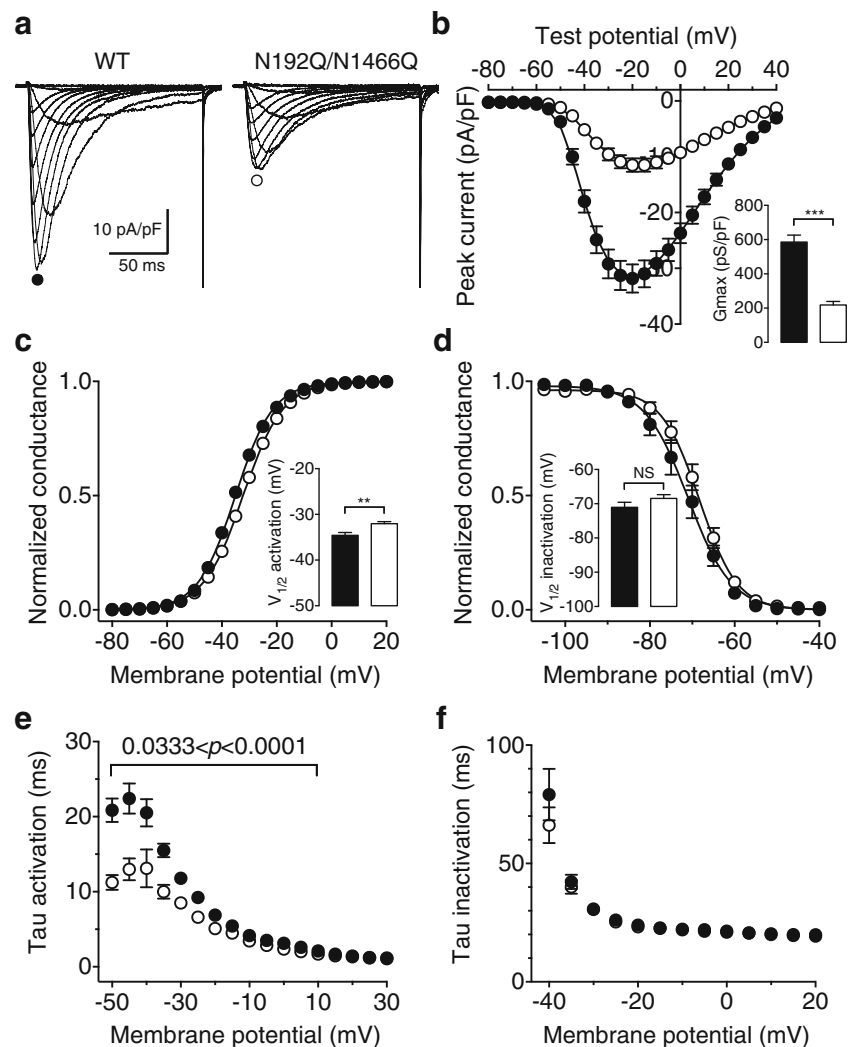
Glycosylation of hCa_v3.2 at asparagine residues N192 and N1466 was further analyzed biochemically by western blot. Glycosylation-deficient channels are anticipated to present a lower molecular weight expected to result in a gel shift in SDS-PAGE. However, and consistent with previous reports [23, 37], glycosylation-deficient channels virtually run at the same molecular weight as the wild-type channel (data not shown), likely due to the high molecular weight of the channel

protein that does not provide enough resolution to visualize changes of few kilodaltons expected when disrupting a glycosylation site. To by pass this technical issue, we generated cDNA constructs encoding only for amino-terminal Myc-tagged transmembrane domains I (residues 51 to 464) and III (residues 1212 to 1586) of hCa_v3.2 that contain asparagine residues N192 and N1466, respectively (Fig. 2a). Western blot analyses using an anti-Myc antibody of Myc-tagged hCa_v3.2 domains expressed in tsA-201 cells revealed a significant gel shift of the glycosylation-deficient domain III (DIII N1466Q) compared to the wild-type domain (Fig. 2b, top panel). This result is consistent with the notion that glycosylation occurs at asparagine N1466 (Fig. 2b, top panel). Surprisingly, we were not able to detect expression of the Myc-tagged domain I using an anti-Myc antibody, possibly due to a proteolytic cleavage of the tag (Fig. 2b, top panel). In contrast, taking advantage of the additional exofacial HA tag, expression of the domain I was revealed using an anti-HA antibody (Fig. 2b, bottom panel). In contrast to the domain III, virtually no change in the electrophoretic mobility of the glycosylation-

deficient domain I (DI N192Q) was observed. Considering that preventing glycosylation at asparagine N192 had a significant functional influence on the surface expression of the channel protein, one possible explanation is that glycosylation at this locus does not occur when the domain I is expressed alone, or that the structure of the glycan is different from the one in domain III.

Finally, to further evaluate whether N-glycosylation at asparagine residues N192 and N1466 have additional roles besides controlling expression of the channel protein, we performed patch-clamp recordings of hCa_v3.2 channels expressed in tsA-201 cells to assess some of the main biophysical properties of the channel. Representative current traces in response to 150-ms depolarizing steps to values ranging -80 and $+30$ mV, from a holding potential of -100 mV, are shown in Fig. 3a for wild-type and glycosylation-deficient N192Q/N1466Q hCa_v3.2 channels. Consistent with our observation that surface expression of N192Q/N1466Q mutant channels is reduced, T-type currents recorded from cells expressing the glycosylation-deficient channel were found to be significantly reduced compared to cells

Fig. 3 Biophysical properties of glycosylation-deficient hCa_v3.2 channels. **a** Representative Ba²⁺ current traces recorded in response to 150-ms depolarization steps to values ranging between -80 and $+30$ mV, from a holding potential of -100 mV, for wild-type hCa_v3.2 and glycosylation-deficient N192Q/N1466Q channels. **b** Corresponding mean current-voltage relationship for hCa_v3.2 WT (filled circles, $n = 46$) and N192Q/N1466Q channels (open circles, $n = 46$). Inset represents the respective maximal conductance. **c** Mean normalized voltage dependence of the macroscopic Ba²⁺ conductance. Inset represents the corresponding mean half-activation potentials. **d** Mean normalized voltage dependence of steady-state inactivation for WT (filled circles, $n = 14$) and N192Q/N1466Q channels (open circles, $n = 13$). Inset represents the corresponding mean half-steady-state inactivation potentials. **e** Time constant of current activation for WT (filled circles, $n = 18$) and N192Q/N1466Q channels (open circles, $n = 19$). **f** Time constant of current inactivation



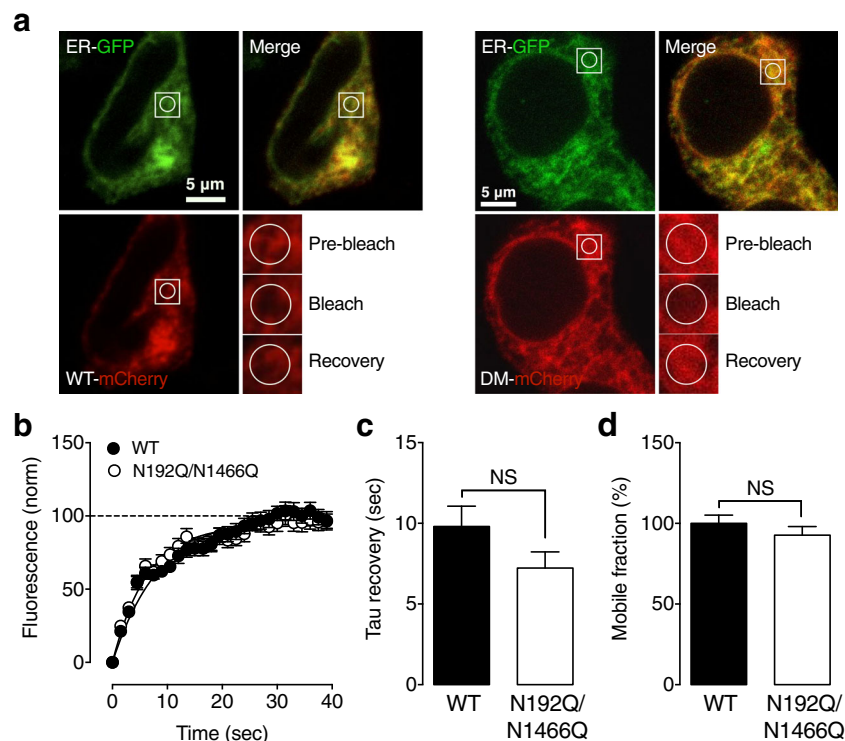


Fig. 4 Intracellular mobility of hCa_v3.2 channels in the endoplasmic reticulum. **a** Representative confocal images of live tsA-201 cells expressing WT (*left panels*) and glycosylation-deficient N192Q/N1466Q (double mutant, DM) mCherry-tagged hCa_v3.2 channels (*red*) together with the ER-targeted GFP (*green*). *Insets* show a magnification of the region of interest before (pre-bleach), immediately after (bleach), and 40 s after (recovery) photobleaching of mCherry-tagged channels. **b** Corresponding mean normalized recovery of fluorescence for WT (*filled*

circles, $n = 18$) and N192Q/N1466Q hCa_v3.2 channels (*open circles*, $n = 21$). **c** Corresponding time constant of fluorescence recovery kinetics for WT (*filled bars*) and N192Q/N1466Q hCa_v3.2 channels (*open bars*). **d** Corresponding mean normalized mobile fraction of WT (*filled bars*) and N192Q/N1466Q hCa_v3.2 channels (*open bars*). Data are presented as mean \pm S.E.M and analyzed by Student's unpaired t tests: NS non statistically significant

expressing the wild-type channel (Fig. 3b). For instance, in response to a depolarizing pulse to -20 mV, the mean peak current density was decreased by 64 % ($p < 0.0001$) in cells expressing the glycosylation-deficient channel (-11.5 ± 1.2 pA/pF, $n = 46$) compared to cells expressing the WT channel (-31.8 ± 1.5 pA/pF, $n = 46$). The maximal conductance was reduced by 63 % ($p < 0.0001$) in cells expressing the N192Q/N1466Q channel mutant (218.6 ± 20.4 pS/pF, $n = 46$) compared to cells expressing the WT channel (585.4 ± 41.2 pS/pF, $n = 46$) (Fig. 3b, inset). We also determined the voltage dependence of the T-type current activation. A mild shift of the mean half-activation potential toward more depolarized potentials by 2.5 mV ($p = 0.0027$) was observed in cells expressing the glycosylation-deficient channel (-32.04 ± 0.44 mV, $n = 46$) compared to cells expressing the WT channel (-34.58 ± 0.63 mV, $n = 46$) (Fig. 3c). In contrast, the voltage dependence of steady-state inactivation remained unaffected (-71.05 ± 1.46 mV, $n = 46$ for WT channels, and -68.45 ± 1.11 mV, $n = 46$ for N192Q/N1466Q channels) (Fig. 3d). Finally, the activation and inactivation kinetics of hCa_v3.2 channels were analyzed by fitting individually the developing and decay phases of the T-type current with a single exponential function. We found that T-type current activation

was slightly accelerated in cells expressing the glycosylation-deficient channel, especially at lower voltages (Fig. 3e). In contrast, there was no significant difference in the inactivation time constant between the WT and N192Q/N1466Q mutant channel (Fig. 3f).

Altogether, these data indicated that glycosylation of hCa_v3.2 at asparagine residues N192 and N1466 has little effect on the macroscopic biophysical properties of the channel and essentially controls surface expression of the channel protein.

N-glycosylation stabilizes expression of hCa_v3.2 channels at the cell surface

The steady-state expression of T-type channels at the cell surface is the net result between the number of channels arriving at and being removed from the plasma membrane. To analyze whether N-linked glycosylation affects the intracellular forward trafficking of T-type channels, we performed fluorescence recovery after photobleaching (FRAP) at physiological temperature (37 °C) in live tsA-201 cells expressing mCherry-tagged hCa_v3.2 channels.

To assess the mobility of the channel protein in the endoplasmic reticulum and in the Golgi apparatus, cells were co-transfected either with an ER-targeted (ER-GFP) (Fig. 4a) or Golgi-targeted (Golgi-GFP) (Fig. 5a) green fluorescent protein (GFP) in order to select the respective region of interest (ROI) for FRAP experiments. Our FRAP measurements indicate that ER trafficking of the glycosylation-deficient N192Q/N1466Q mutant channel is unaffected compared to the wild-type channel (Fig. 4b–d). A similar result was observed in the Golgi apparatus although a non-significant tendency to a decreased mobile fraction was observed for the N192Q/N1466Q mutant (Fig. 5b–d), indicating that glycosylation at asparagine residues N192 and N1466 has little influence on the intracellular forward trafficking of hCa_v3.2 channels to the cell surface.

To further analyze the role of N-glycosylation in the expression of T-type channels at the cell surface, we conducted internalization measurements of HA-hCa_v3.2 channels in live tsA-201 cells at 37 °C. At $t = 0$ before any internalization has occurred yet, the surface expression of the wild-type HA-hCa_v3.2 was evidenced by

immunostaining signal in non-permeabilized cells, while intracellular staining was absent from permeabilized cells (Fig. 6a, left panels). In contrast, after 180 min at 37 °C, internalization of the channel protein was clearly evidenced by a clear intracellular immunoreactivity of permeabilized cells, while surface expression of the channel was virtually undetectable (Fig. 6a, right panels). Analysis of the internalization kinetics indicated that the time constant of internalization of the glycosylation-deficient N192Q/N1466Q hCa_v3.2 channel is three times faster ($p = 0.0261$) ($\tau = 38.3 \pm 5.9$ min, $n = 3$) compared to the wild-type channel ($\tau = 115.6 \pm 20.5$ min, $n = 4$) (Fig. 6b, c). Remarkably, the internalization data appeared to be proportionally correlated with the steady-state expression of the channel at the plasma membrane in Fig. 1, suggesting the possibility that the difference in cell surface expression between the glycosylation-deficient N192Q/N1466Q channel and the WT channel is mediated by a differential stability of the channel protein at the cell surface.

Altogether, these data indicate that N-glycosylation of hCa_v3.2 channels at asparagine residues N192 and

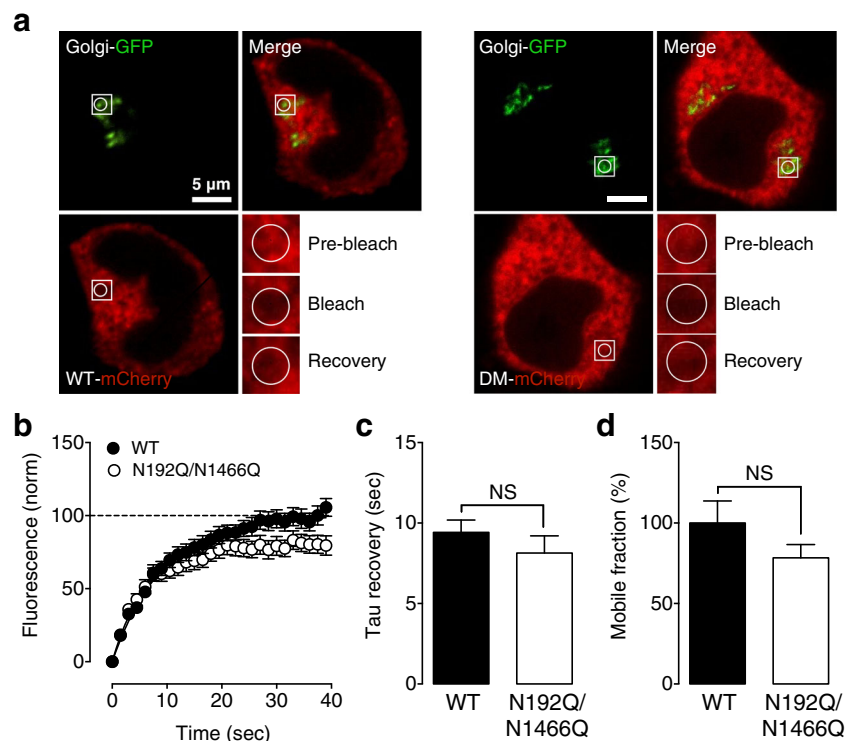


Fig. 5 Intracellular mobility of hCa_v3.2 channels in the Golgi apparatus. **a** Representative confocal images of live tsA-201 cells expressing WT (left panels) and glycosylation-deficient N192Q/N1466Q (double mutant, DM) mCherry-tagged hCa_v3.2 channels (red) together with the Golgi-targeted GFP (green). Insets show a magnification of the region of interest before (pre-bleach), immediately after (bleach), and 40 s after (recovery) photobleaching of mCherry-tagged channels. **b** Corresponding mean normalized recovery of fluorescence for WT

(filled circles, $n = 21$) and N192Q/N1466Q hCa_v3.2 channels (open circles, $n = 19$). **c** Corresponding mean time constant of fluorescence recovery kinetics for WT (filled bars) and N192Q/N1466Q hCa_v3.2 channels (open bars). **d** Corresponding mean normalized mobile fraction of WT (filled bars) and N192Q/N1466Q hCa_v3.2 channels (open bars). Data are presented as mean \pm S.E.M and analyzed by Student's unpaired t tests: NS non statistically significant

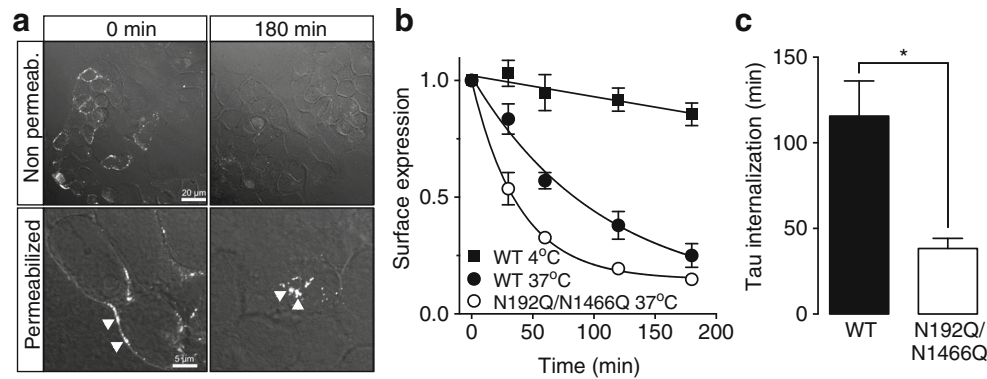


Fig. 6 N-glycosylation stabilizes hCa_v3.2 channels at the plasma membrane. **a** Representative confocal images of non-permeabilized (top panels) and permeabilized (bottom panels) tsA-201 cells expressing HA-hCa_v3.2 channels and live immunostained with a primary anti-HA antibody before internalization (0 min, left panels) and after 180-min internalization (180 min, right panels) of the channel at 37 °C. Arrows indicate surface channels before internalization (permeabilized, left panel) and internalized channels (permeabilized, right panel). **b** Corresponding mean internalization kinetics assessed by monitoring the

time-dependent surface expression of WT (filled circles, $n = 4$) and N192Q/N1466Q hCa_v3.2 channels (open circles, $n = 3$). Internalization kinetics of the WT hCa_v3.2 channels measured at 4 °C is also shown (filled squares, $n = 3$). Each measurement was obtained by averaging the fluorescence intensity of 10 confocal fields from independent experiments. **c** Corresponding time constant of internalization kinetics for WT (filled bar) and N192Q/N1466Q hCa_v3.2 channels (open bar). Data are presented as mean \pm S.E.M and analyzed by Student's unpaired t tests: * $p < 0.05$

N1466 has little influence on the intracellular forward trafficking of the channel to the cell surface, but is essential for the stability of the channel protein in the plasma membrane.

Extracellular glucose level modulates surface expression of hCa_v3.2 channels

We have previously proposed that N-glycosylation of hCa_v3.2 channels might support a glucose-dependent potentiation of T-type calcium currents, which may play an important role in the sensitization of primary nociceptive neurons during mellitus diabetes [37]. However, whether external glucose affects the functioning of hCa_v3.2 or the expression of the channel protein at the cell surface remains unknown. To further assess the role of external glucose, we assessed the expression of hCa_v3.2 channels in physiological (5 mM glucose), hypoglycemic (2 mM) and hyperglycemic (diabetic-like) conditions (15 and 25 mM), under identical osmolarity. Immunostaining of HA-hCa_v3.2 channels from non-permeabilized cells revealed a direct correlation between the external glucose levels and the expression of the channel protein at the cell surface. For instance, the cell surface expression of wild-type hCa_v3.2 was decreased by 0.4-fold ($p = 0.0211$) in cells maintained in reduced glucose condition (2 mM) compared to cells maintained under physiological glucose level (5 mM) (Fig. 7b). In contrast, the surface expression of hCa_v3.2 was found significantly increased by 1.8-fold (15 mM, $p = 0.0005$) and 1.7-fold (25 mM, $p < 0.0002$) in cells exposed to elevated glucose levels (Fig. 7a, b, right panels). Because the effect of external glucose levels on

the expression of the channel protein at the cell surface could have resulted from an altered protein production, we assessed the total expression of hCa_v3.2 channels by immunostaining. Under reduced and elevated glucose conditions, the total expression of the channel proteins assessed from permeabilized cells remained unchanged compared to physiological glucose levels (Fig. 7a, b, left panels), indicating that the differential surface expression of hCa_v3.2 channels under various glucose levels likely resulted from an alteration of the trafficking and/or stability of the channel protein at the plasma membrane. This notion is further supported by the observation that the surface and total expression of a non-glycosylated “mock” membrane-targeted GFP (LcK-GFP) was unaffected in elevated glucose conditions, ruling out an indirect effect of high glucose levels on the overall functioning of the cell machinery which may have affected the general expression and trafficking of proteins (Fig. 7c, d).

In another set of experiments, we assessed the role of glycosylation in the glucose-dependent modulation of hCa_v3.2 channel expression. Immunostaining of HA-hCa_v3.2 channels from non-permeabilized cells revealed a 2.3-fold increased ($p = 0.0133$) surface expression of the wild-type channel in cells maintained in elevated glucose condition (25 mM) (Fig. 7e, right panel). In contrast, the surface expression of the glycosylation-deficient N192Q/N1466Q mutant channel remained unaltered suggesting that proper N-glycosylation of the channel protein is required to support glucose-dependent potentiation of T-type channel expression. In addition, internalization measurements of hCa_v3.2 channels at 37 °C under elevated glucose conditions was unaltered, suggesting that the increased T-type channel expression at the cell surface in elevated glucose conditions likely

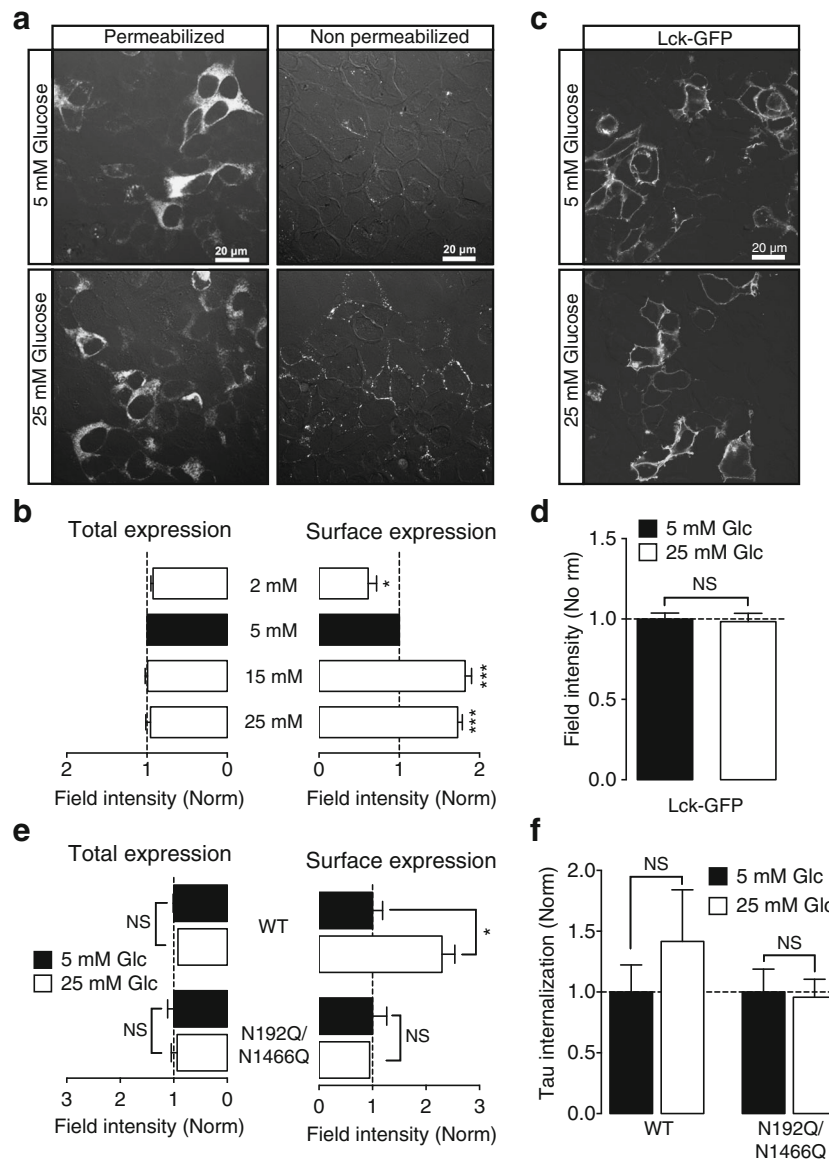


Fig. 7 External glucose level modulates surface expression of hCa_v3.2 channels. **a** Low-magnification confocal images of permeabilized (*left panels*) and non-permeabilized (*right panels*) tsA-201 cells expressing WT HA-hCa_v3.2 channels maintained under physiological (5 mM, *top panels*) and elevated glucose levels (25 mM, *bottom panels*) and immunostained using a primary anti-HA antibody. **b** Corresponding mean total (permeabilized) and surface (non-permeabilized) expression of WT hCa_v3.2 channels in physiological (*filled bars*, *n* = 3) and various glucose levels (*open bars*, *n* = 3) assessed by field fluorescence intensity measurement. Each measurement was obtained by averaging the fluorescence intensity of 10 confocal fields from independent experiments. **c** Low-magnification confocal images of live tsA-201 cells

expressing a plasma membrane-GFP (Lck-GFP) maintained under physiological (*top panel*) and elevated glucose levels (*bottom panel*). **d** Corresponding mean expression of Lck-GFP in physiological (*filled bar*, *n* = 3) and elevated glucose condition (*open bar*, *n* = 3). **e** Mean total and surface expression of WT and N192Q/N1466Q hCa_v3.2 channels in physiological (5 mM) (*filled bars*, *n* = 3) and elevated (25 mM) glucose conditions (*open bars*, *n* = 3). **f** Time constant of internalization at 37 °C of WT and N192Q/N1466Q HA-hCa_v3.2 in physiological (*filled bars*, *n* = 3) and elevated glucose levels (*open bars*, *n* = 3). Data are presented as mean ± S.E.M and analyzed by Student's unpaired *t* tests: NS non statistically significant; **p* < 0.05

resulted from an increased forward trafficking of the channel to the plasma membrane (Fig. 7f).

Altogether, these results indicate that the expression of hCa_v3.2 channels at the plasma membrane is controlled by external glucose concentration, and that glucose-dependent expression of hCa_v3.2 at the cell surface relies on the glycosylation of the channel protein.

External glucose concentration increases forward trafficking of hCa_v3.2 channels

To further examine the role of external glucose in the trafficking of T-type channels, we performed FRAP measurements at physiological temperature to assess the mobility of hCa_v3.2 channels in physiological and high

glucose conditions. FRAP measurements in the ER revealed a 26 % increase ($p = 0.0494$) in the mobile fraction for the wild-type channel under elevated glucose conditions compared to physiological glucose levels (Fig. 8a, d). The time constant of recovery was found slightly slowed down ($p = 0.0013$) in high glucose ($\tau = 9.8 \pm 0.9$ s, $n = 19$) compared to low glucose conditions ($\tau = 6.0 \pm 0.5$ s, $n = 17$), which may have resulted from the saturation of the trafficking machinery (Fig. 8c). Similarly, FRAP measurements in the Golgi apparatus showed a 25 % increase ($p = 0.0212$) in the mobile fraction for the wild-type hCa_v3.2 channel (Fig. 8e, h) while the kinetics of recovery in high glucose conditions remained unchanged compared to physiological glucose level ($\tau = 10.3 \pm 1.2$ s, $n = 24$, versus $\tau = 10.1 \pm 1.3$ s, $n = 23$, respectively) (Fig. 8g). In contrast, and consistent with the notion that glucose-dependent potentiation of hCa_v3.2 relies on the glycosylation of the channel protein, elevated external glucose level had no effect on the intracellular dynamic of the glycosylation-deficient N192Q/N1466Q mutant channel, both in the ER (Fig. 8b–d) and in the Golgi apparatus (Fig. 8f–h).

Collectively, these results indicate that elevated external glucose levels specifically potentiates intracellular forward trafficking of hCa_v3.2 without affecting channel surface stability, and requires glycosylation at asparagine residues N192 and N1466.

External glucose level modulates the low-threshold calcium conductance in DRG neurons

To further assess the importance of external glucose on T-type channel expression in a more physiological context, we analyzed the effect of elevated external glucose levels on T-type channel-mediated calcium entry into primary rat DRG neurons in culture. Acutely dissociated DRG neurons maintained under elevated (25 mM) glucose condition for 48 h were loaded with the calcium indicator dye Fluo-4 and high-voltage activated calcium channels were blocked with 10 μ M cadmium and cells were depolarized with application of 50 mM KCl to trigger T-type channel-mediated calcium influx. Consistent with our observation that surface expression of T-type channels is increased under elevated glucose conditions, calcium imaging experiments revealed a significant increase of the low-threshold calcium influx in DRG neurons maintained in elevated glucose condition. For instance, the integral of the Fluo-4 signal during the calcium rising phase was significantly increased ($p = 0.0323$) in elevated glucose conditions (6.7 ± 0.4 DF/F0.sec, $n = 52$) compared to physiological glucose levels (5.2 ± 0.5 DF/F0.sec, $n = 52$) (Fig. 9a, b).

Altogether, these experiments reveal that elevated external glucose levels potentiate T-type channel expression in DRG neurons, which may have important implications in the

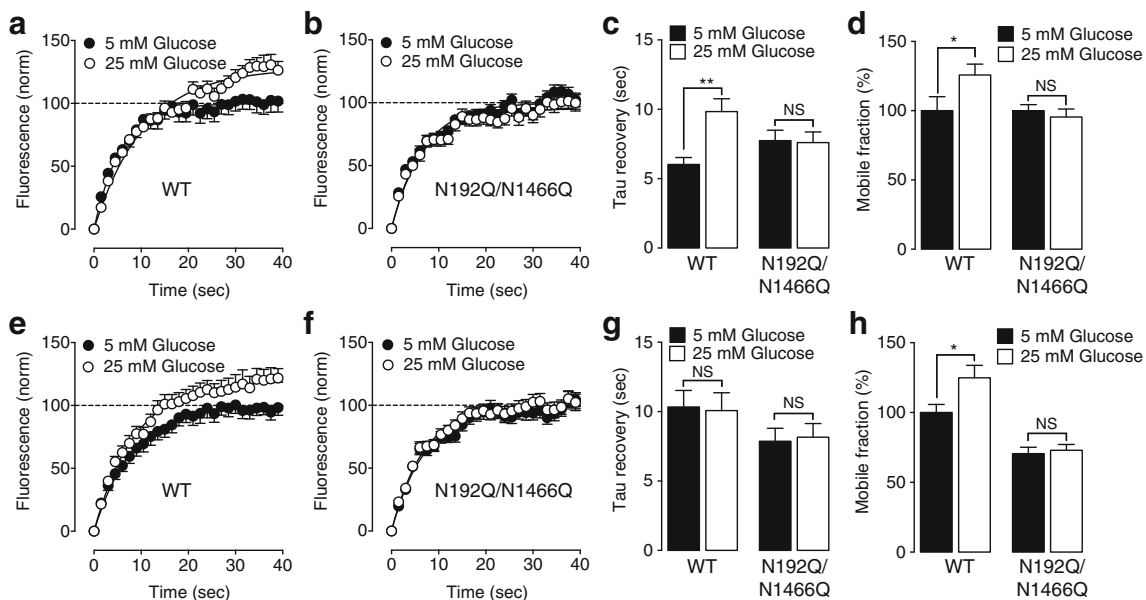


Fig. 8 Elevated external glucose level increases forward trafficking of hCa_v3.2 channels. **a** Mean normalized recovery of fluorescence after bleaching for WT mCherry-hCa_v3.2 channels measured in the endoplasmic reticulum in physiological (filled circles, $n = 23$) and elevated glucose conditions (open circles, $n = 23$). **b** Same as earlier (**a**) but for glycosylation-deficient N192Q/N1466Q mCherry-hCa_v3.2 channels in regular (filled circles, $n = 25$) and elevated glucose (open circles, $n = 25$). **c** Corresponding mean time constant of fluorescence

recovery for WT and N192Q/N1466Q hCa_v3.2 channels in physiological (filled bars) and elevated glucose conditions (open bars). **d** Corresponding mean normalized mobile fraction for WT and N192Q/N1466Q hCa_v3.2 channels in physiological (filled bars) and elevated glucose conditions (open bars). **e–h** Same as earlier (**a–d**) but measured in the Golgi apparatus. Data are presented as mean \pm S.E.M and analyzed by Student's unpaired *t* tests. NS non statistically significant; * $p < 0.05$; ** $p < 0.01$

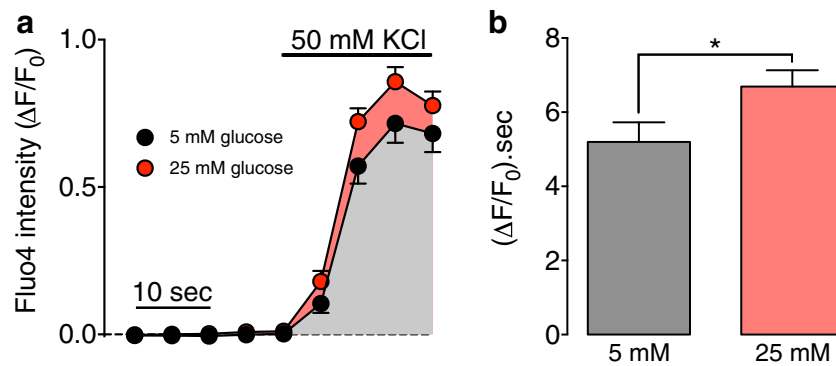


Fig. 9 External glucose regulates T-type channel expression in DRG neurons. **a** Mean Fluo-4 signal triggered by application of 50 mM KCl in primary rat DRG neurons maintained under physiological (5 mM,

black circles, $n = 52$) and elevated (25 mM, red circles, $n = 52$) glucose conditions. **b** Corresponding mean integral of the fluorescence signal measured during the time course of the rising phase of the calcium influx

context of peripheral painful diabetic neuropathy where the increased expression of T-type channels is believed to be at the origin of the enhanced excitability of these neurons.

Discussion

Alteration of T-type channel expression was proposed to be causally related to the development of peripheral painful diabetic neuropathy [8], and previous reports have documented a role for glucose and N-linked glycosylation in the expression of T-type channels [37] [23]. Here, we show that although N-glycosylation of hCa_v3.2 and external glucose levels differentially affect the fate of the channel protein, they act in concert

to control the expression of T-type channels at the cell surface. While elevated external glucose levels potentiate intracellular forward trafficking of the channel to the cell surface, site-specific N-glycosylation of hCa_v3.2 is essential to stabilize expression of T-type channels at the plasma membrane (Fig. 10).

To assess the role of N-linked glycosylation in the expression of T-type channels, we used glycosylation-deficient hCa_v3.2 channels where canonical glycosylation motifs were disrupted by replacing asparagine residues with glutamine residues. Consistent with previous study using different assays [23, 37], we showed by surface immunostaining of HA-tagged hCa_v3.2 that disrupting N-glycosylation at any loci caused a significant reduction

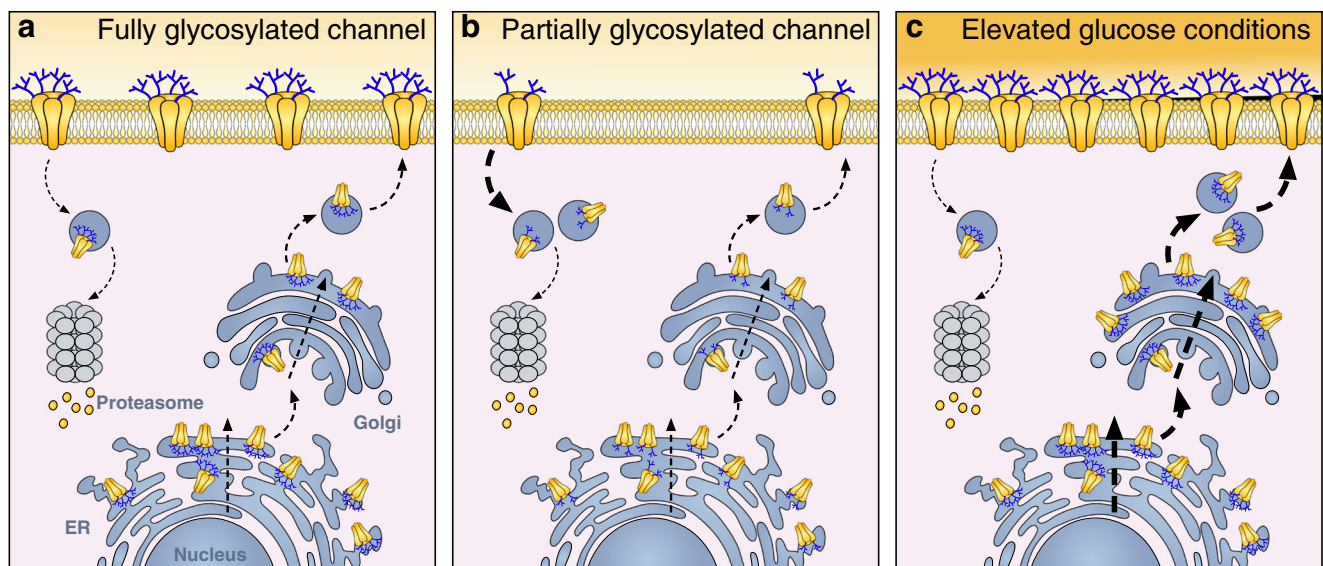


Fig. 10 Graphical summary of the effect of glucose and N-glycosylation on the expression of hCa_v3.2 channels. **a** In physiological conditions, hCa_v3.2 channels are fully glycosylated and traffic to the cell surface through the ER and Golgi apparatus. The steady-state expression of the channel results from the amount of channel proteins coming to and getting internalized from the plasma membrane. **b** Upon disruption of asparagine residues N192 and N1466, partially glycosylated channels

traffic to the plasma membrane but get internalized faster compared to fully glycosylated channels, causing a decreased surface expression of the channel proteins at the cell surface. **c** Under elevated external glucose levels, the trafficking of hCa_v3.2 channels to the cell surface is increased while their internalization rate remains unaffected, causing an increased expression of the channel protein at the plasma membrane

of the expression of T-type channels at the cell surface. We observed that preventing glycosylation at asparagine residues N271 and N1710 caused a drastic reduction of the total expression of the channel protein, which is likely responsible for the decreased expression of these channel mutants at the plasma membrane. It is conceivable that glycosylation at asparagine residues N271 and N1710 is required for calnexin/calreticulin-dependent quality control of newly synthesized glycoproteins that occurs in the ER [26]. In contrast, the decreased surface expression of glycosylation-deficient N192Q and N1466Q channels, and so the double N192Q/N1466Q mutant channel was not associated with any alteration of the total protein expression, suggesting that glycosylation at these specific loci may contribute to the trafficking of the channel. Therefore, we have used the N192Q/N1466Q hCa_v3.2 mutant as the minimal glycosylated channel to further assess the role of N-linked glycosylation in the trafficking of T-type channels. The steady-state expression of T-type channels at the cell surface is the net consequence between the number of channel proteins arriving at and being removed from the plasma membrane. Our internalization studies of hCa_v3.2 channels performed at physiological temperature revealed that preventing glycosylation at asparagine residues N192 and N1466 drastically decreased the stability of the channel at the cell surface. In contrast, the forward trafficking of the glycosylation-deficient N192Q/N1466Q channel assessed by FRAP measurement in the ER and Golgi apparatus was not affected, indicating that N-linked glycosylation of hCa_v3.2 potentiates surface expression of the T-type channel by stabilizing the channel protein at the plasma membrane. This notion is consistent with previous studies showing that N-glycosylation stabilizes CIC-5 and K_v1.3 channels at the cell surface [30, 44]. Although the underlying mechanisms by which N-glycosylation stabilizes channel protein at the plasma membrane remain elusive, it was proposed that binding of the N-glycan attached to the channel protein with extracellular lectin proteins might stabilize surface expression of the channel. For instance, it was demonstrated that klotho-dependent removal of sialic acid moieties from TRPV5 channels exposes the N-glycan tree attached to the channel to interact with galactin proteins thus decreasing dynamin-dependent internalization of the channel [15, 41]. In addition, it was reported that N-glycosylation contributes to plasma membrane compartmentalization of proteins into subdomains. Indeed, it was reported that fully (complex)-glycosylated TRPM8 channels essentially distribute into lipid rafts, whereas core-glycosylated or glycosylation-deficient mutant channels are randomly distributed in the plasma membrane [19]. Hence, glycosylation-dependent control of sub-plasma membrane localization of ion channels

may play an important role in the stability of the channel at the cell surface. This notion is supported by biochemical studies on pancreatic beta cells showing that preventing N-glycosylation of the glucose transporter GLUT2 led to a redistribution of the transporter into lipid rafts and the increased internalization of the protein [20, 21].

Given that N-glycosylation is an essential post-translational modification that contributes to the expression of T-type channels, alteration of the glycosylation machinery and/or availability of monosaccharides that serve as building blocks of the glycan tree may have important consequences on the expression of the channel protein. Hence, in a second set of experiments, we have analyzed the role of external glucose concentration in the expression of hCa_v3.2 channels. Consistent with our previous study showing a glucose-dependent potentiation of the T-type calcium conductance [37], our data revealed that elevated external glucose concentration caused a significant increase of the expression of the channel protein at the cell surface, without affecting the total expression of the channel. This observation is consistent with previous results obtained with two-pore domain potassium (K2P) channels showing that elevated glucose levels potentiate surface expression of the channel [17]. In contrast, surface expression of the glycosylation-deficient N192Q/N1466Q mutant channel was not influenced by external glucose levels, suggesting that glucose-dependent potentiation of hCa_v3.2 channels requires the presence of the glycan tree on the channel protein. However, in contrast to N-glycosylation that stabilized the channel protein at the plasma membrane, our internalization studies indicated that external glucose levels has no influence on the stability of the channel at the cell surface. In contrast, we showed that increasing external glucose levels potentiates the intracellular forward trafficking of the channel. These results suggest that under elevated glucose conditions, a larger pool of channel proteins is able to traffic through the ER and Golgi apparatus, which eventually may contribute to the elevated surface expression of the channel. It is conceivable that external glucose may influence the structure and/or composition of the glycan tree attached to the channel and impacting the mobility of the protein. This notion is supported by recent studies showing that decreased external glucose concentration is associated with a decreased availability of a number of glycosylation precursors and altered N-glycan structures of monoclonal antibodies [16, 35]. In addition, glucose-dependent variation of the glycan structure can also result from altered activity of enzymes involved in the glycosylation pathway. For instance, increased activity of glycan processing enzymes was reported *in vitro* and *in vivo* in animal models of diabetes [25]. Considering

that N-glycans can serve as signals to control the sorting of proteins, altered structure and/or composition of the oligosaccharide in elevated glucose conditions may be responsible for the increased trafficking of hCa_v3.2 channels. This notion is supported by previous results showing that bisecting N-glycans of SREC-I receptor promotes intracellular trafficking of the receptor to the cell surface [28]. It is worth mentioning that although elevated glucose levels caused an increased mobile fraction of hCa_v3.2 channels, the mobility kinetic was in contrast reduced. Since in high glucose condition glycosylation site occupancy can be increased, a slower mobility rate may have resulted from an increased channel interaction with lectin chaperons such as calnexin, which would slow down the dynamics of the channel.

Although further studies will be needed to uncover the detailed underlying molecular mechanisms by which glucose and N-glycosylation control expression of T-type channels, our observation that the external glucose level acts in concert with N-glycosylation to potentiate surface expression of hCa_v3.2 channels represents an intriguing mechanism of physio (patho) logical importance, especially for cells that lack the insulin-regulated glucose transporter GLUT4. For instance, it was reported that elevated extracellular glucose concentration leads to increased intracellular glucose levels [5, 33], and increased production of UDP-N-acetylglucosamine (UDP-GlcNAc) via the hexosamine pathway that serves as a substrate for N-glycosylation [1, 13, 29]. In addition, increased levels of dolichol (the membrane anchor from which the precursor oligosaccharide is transferred to the protein) and protein glycosylation were reported in animal models of diabetes [2]. All of these aspects further support the notion that hyperglycemia can enhance glycosylation of proteins.

In summary, our data provided compelling evidence for a cooperative role of glucose and glycosylation in the control of T-type channel expression at the plasma membrane. This may be potentially of high relevance in the development of painful peripheral pain arising from diabetic conditions. Further studies to characterize the cellular molecules involved in this process may unveil important new targets that could be of potential interest for therapeutic purposes.

Acknowledgments We are grateful to Drs. Michael E. Daily and Steven H. Green (University of Iowa) for providing the LcK-GFP construct.

Compliance with ethical standards

Conflict of interest The authors declare that they have no conflict of interest.

Financial support Work in the Weiss laboratory is supported by the Czech Science Foundation (grant 15-13556S), the Czech Ministry of

Education Youth and Sports (grant 7AMB15FR015), and the Institute of Organic Chemistry and Biochemistry (IOCB). Y.R. and J.L. are supported by an IOCB postdoctoral fellowship.

References

- Anagnostou SH, Shepherd PR (2008) Glucose induces an autocrine activation of the Wnt/beta-catenin pathway in macrophage cell lines. *Biochem J* 416(2):211–218
- Bar-On H, Neshet G, Teitelbaum A, Ziv E (1997) Dolichol-mediated enhanced protein N-glycosylation in experimental diabetes—a possible additional deleterious effect of hyperglycemia. *J Diabetes Complicat* 11(4):236–242
- Beurrier C, Congar P, Bioulac B, Hammond C (1999) Subthalamic nucleus neurons switch from single-spike activity to burst-firing mode. *J Neurosci* 19(2):599–609
- Cain SM, Snutch TP (2013) T-type calcium channels in burst-firing, network synchrony, and epilepsy. *Biochim Biophys Acta* 1828(7):1572–1578
- Campos C (2012) Chronic hyperglycemia and glucose toxicity: pathology and clinical sequelae. *Postgrad Med* 124(6):90–97
- Crunelli V, Cope DW, Hughes SW (2006) Thalamic T-type Ca²⁺ channels and NREM sleep. *Cell Calcium* 40(2):175–190
- Dubel SJ, Altier C, Chaumont S, Lory P, Bourinet E, Nargeot J (2004) Plasma membrane expression of T-type calcium channel alpha(1) subunits is modulated by high voltage-activated auxiliary subunits. *J Biol Chem* 279(28):29263–29269
- Duzhyy DE, Viatchenko-Karpinski VY, Khomula EV, Voitenko NV, Belan PV (2015) Upregulation of T-type Ca²⁺ channels in long-term diabetes determines increased excitability of a specific type of capsaicin-insensitive DRG neurons. *Mol Pain* 11:29
- García-Caballero A, Gadotti VM, Stenkowski P, Weiss N, Souza IA, Hodgkinson V, Bladen C, Chen L, Hamid J, Pizzoccaro A, Deage M, François A, Bourinet E, Zamponi GW (2014) The deubiquitinating enzyme USP5 modulates neuropathic and inflammatory pain by enhancing Cav3.2 channel activity. *Neuron* 83(5):1144–1158
- Jagodic MM, Pathirathna S, Joksovic PM, Lee W, Nelson MT, Naik AK, Su P, Jevtovic-Todorovic V, Todorovic SM (2008) Upregulation of the T-type calcium current in small rat sensory neurons after chronic constrictive injury of the sciatic nerve. *J Neurophysiol* 99(6):3151–3156
- Jagodic MM, Pathirathna S, Nelson MT, Mancuso S, Joksovic PM, Rosenberg ER, Bayliss DA, Jevtovic-Todorovic V, Todorovic SM (2007) Cell-specific alterations of T-type calcium current in painful diabetic neuropathy enhance excitability of sensory neurons. *J Neurosci* 27(12):3305–3316
- Latham JR, Pathirathna S, Jagodic MM, Choe WJ, Levin ME, Nelson MT, Lee WY, Krishnan K, Covey DF, Todorovic SM, Jevtovic-Todorovic V (2009) Selective T-type calcium channel blockade alleviates hyperalgesia in Ob/Ob mice. *Diabetes* 58(11):2656–2665
- Lau KS, Partridge EA, Grigorian A, Silvescu CI, Reinhold VN, Demetriou M, Dennis JW (2007) Complex N-glycan number and degree of branching cooperate to regulate cell proliferation and differentiation. *Cell* 129(1):123–134
- Lazniewska J, Weiss N (2014) The “sweet” side of ion channels. *Rev Physiol Biochem Pharmacol* 167:67–114
- Leunissen EH, Nair AV, Büll C, Lefeber DJ, van Delft FL, Bindels RJ, Hoenderop JG (2013) The epithelial calcium channel TRPV5 is

- regulated differentially by klotho and sialidase. *J Biol Chem* 288(41):29238–29246
16. Liu B, Spearman M, Doering J, Lattová E, Perreault H, Butler M (2014) The availability of glucose to CHO cells affects the intracellular lipid-linked oligosaccharide distribution, site occupancy and the N-glycosylation profile of a monoclonal antibody. *J Biotechnol* 170:17–27
 17. Mant A, Williams S, Roncoroni L, Lowry E, Johnson D, O’Kelly I (2013) N-glycosylation-dependent control of functional expression of background potassium channels K2P3.1 and K2P9.1. *J Biol Chem* 288(5):3251–3264
 18. Moremen KW, Tiemeyer M, Nairn AV (2012) Vertebrate protein glycosylation: diversity, synthesis and function. *Nat Rev Mol Cell Biol* 13(7):448–462
 19. Morenilla-Palao C, Pertusa M, Meseguer V, Cabedo H, Viana F (2009) Lipid raft segregation modulates TRPM8 channel activity. *J Biol Chem* 284(14):9215–9224
 20. Ohtsubo K, Takamatsu S, Gao C, Korekane H, Kurosawa TM, Taniguchi N (2013) N-glycosylation modulates the membrane sub-domain distribution and activity of glucose transporter 2 in pancreatic beta cells. *Biochem Biophys Res Commun* 434(2):346–351
 21. Ohtsubo K, Takamatsu S, Minowa MT, Yoshida A, Takeuchi M, Marth JD (2005) Dietary and genetic control of glucose transporter 2 glycosylation promotes insulin secretion in suppressing diabetes. *Cell* 123(7):1307–1321
 22. Ondacova K, Karmazinova M, Lazniewska J, Weiss N, Lacinova L (2016) Modulation of Cav3.2 T-type calcium channel permeability by asparagine-linked glycosylation. *Channels (Austin)* 10(3):175–184
 23. Orestes P, Osuru HP, McIntire WE, Jacus MO, Salajegheh R, Jagodic MM, Choe W, Lee J, Lee SS, Rose KE, Poiri N, Digruccio MR, Krishnan K, Covey DF, Lee JH, Barrett PQ, Jevtovic-Todorovic V, Todorovic SM (2013) Reversal of neuropathic pain in diabetes by targeting glycosylation of Ca (V)3.2 T-type calcium channels. *Diabetes* 62(11):3828–3838
 24. Perez-Reyes E (2003) Molecular physiology of low-voltage-activated t-type calcium channels. *Physiol Rev* 83(1):117–161
 25. Rellier N, Ruggiero-Lopez D, Lecomte M, Lagarde M, Wiernsperger N (1999) In vitro and in vivo alterations of enzymatic glycosylation in diabetes. *Life Sci* 64(17):1571–1583
 26. Roth J, Zuber C, Park S, Jang I, Lee Y, Kysela KG, Le Fourn V, Santimaria R, Guhl B, Cho JW (2010) Protein N-glycosylation, protein folding, and protein quality control. *Mol Cells* 30(6):497–506
 27. Rzhetsky Y, Lazniewska J, Proft J, Campiglio M, Flucher BE, Weiss N (2016) A Cav3.2/Stac1 molecular complex controls T-type channel expression at the plasma membrane. *Channels (Austin)*:1–9
 28. Sano M, Korekane H, Ohtsubo K, Yamaguchi Y, Kato M, Shibukawa Y, Tajiri M, Adachi H, Wada Y, Asahi M, Taniguchi N (2012) N-glycans of SREC-I (scavenger receptor expressed by endothelial cells): essential role for ligand binding, trafficking and stability. *Glycobiology* 22(5):714–724
 29. Schleicher ED, Weigert C (2000) Role of the hexosamine biosynthetic pathway in diabetic nephropathy. *Kidney Int Suppl* 77:S13–S18
 30. Schmieder S, Bogliolo S, Ehrenfeld J (2007) N-glycosylation of the *Xenopus laevis* CIC-5 protein plays a role in cell surface expression, affecting transport activity at the plasma membrane. *J Cell Physiol* 210(2):479–488
 31. Senatore A, Guan W, Spafford JD (2014) Cav3 T-type channels: regulators for gating, membrane expression, and cation selectivity. *Pflugers Arch* 466(4):645–660
 32. Senatore A & Spafford JD (2015). Physiology and pathology of voltage-gated T-type calcium channels. In *T-type Calcium Channels in Basic and Clinical Science* pp. 3–17. Springer,
 33. Tomlinson DR, Gardiner NJ (2008) Glucose neurotoxicity. *Nat Rev Neurosci* 9(1):36–45
 34. Turner RW, Zamponi GW (2014) T-type channels buddy up. *Pflugers Arch* 466(4):661–675
 35. Villacrés C, Tayi VS, Lattová E, Perreault H, Butler M (2015) Low glucose depletes glycan precursors, reduces site occupancy and galactosylation of a monoclonal antibody in CHO cell culture. *Biotechnol J* 10(7):1051–1066
 36. Watanabe M, Ueda T, Shibata Y, Kumamoto N, Shimada S, Ugawa S (2015) Expression and regulation of Cav3.2 T-type calcium channels during inflammatory hyperalgesia in mouse dorsal root ganglion neurons. *PLoS One* 10(5):e0127572
 37. Weiss N, Black SA, Bladen C, Chen L, Zamponi GW (2013) Surface expression and function of Cav3.2 T-type calcium channels are controlled by asparagine-linked glycosylation. *Pflugers Arch* 465(8):1159–1170
 38. Weiss N, Hameed S, Fernández-Fernández JM, Fablet K, Karmazinova M, Poillot C, Proft J, Chen L, Bidaud I, Monteil A, Huc-Brandt S, Lacinova L, Lory P, Zamponi GW, De Waard M (2012) A Ca (v)3.2/syntaxin-1A signaling complex controls T-type channel activity and low-threshold exocytosis. *J Biol Chem* 287(4):2810–2818
 39. Weiss N, Zamponi GW (2013) Control of low-threshold exocytosis by T-type calcium channels. *Biochim Biophys Acta* 1828(7):1579–1586
 40. Weiss N, Zamponi GW, De Waard M (2012) How do T-type calcium channels control low-threshold exocytosis. *Commun Integr Biol* 5(4):377–380
 41. Wolf MT, An SW, Nie M, Bal MS, Huang CL (2014) Klotho up-regulates renal calcium channel transient receptor potential vanilloid 5 (TRPV5) by intra- and extracellular N-glycosylation-dependent mechanisms. *J Biol Chem* 289(52):35849–35857
 42. Yue J, Liu L, Liu Z, Shu B, Zhang Y (2013) Upregulation of T-type Ca²⁺ channels in primary sensory neurons in spinal nerve injury. *Spine (Phila Pa 1976)* 38(6):463–470
 43. Zamponi GW, Striessnig J, Koschak A, Dolphin AC (2015) The physiology, pathology, and pharmacology of voltage-gated calcium channels and their future therapeutic potential. *Pharmacol Rev* 67(4):821–870
 44. Zhu J, Yan J, Thornhill WB (2012) N-glycosylation promotes the cell surface expression of Kv1.3 potassium channels. *FEBS J* 279(15):2632–2644